

## Satellite-based modeling of gross primary production in an evergreen needleleaf forest

Xiangming Xiao<sup>a,\*</sup>, David Hollinger<sup>b</sup>, John Aber<sup>a</sup>, Mike Goltz<sup>c</sup>, Eric A. Davidson<sup>d</sup>,  
Qingyuan Zhang<sup>a</sup>, Berrien Moore III<sup>a</sup>

<sup>a</sup>Complex Systems Research Center, Institute for the Study of Earth, Oceans and Space, University of New Hampshire, Durham, NH 03833, USA

<sup>b</sup>USDA Forest Service, Northeastern Research Station, 271 Mast Road, Durham, NH 03824, USA

<sup>c</sup>Department of Plant, Soil, and Environmental Sciences, University of Maine, Orono, ME 04469, USA

<sup>d</sup>Woods Hole Research Center, P.O. Box 296, Woods Hole, MA 02543, USA

Received 3 March 2003; received in revised form 7 November 2003; accepted 11 November 2003

### Abstract

The eddy covariance technique provides valuable information on net ecosystem exchange (NEE) of CO<sub>2</sub>, between the atmosphere and terrestrial ecosystems, ecosystem respiration, and gross primary production (GPP) at a variety of CO<sub>2</sub> eddy flux tower sites. In this paper, we develop a new, satellite-based Vegetation Photosynthesis Model (VPM) to estimate the seasonal dynamics and interannual variation of GPP of evergreen needleleaf forests. The VPM model uses two improved vegetation indices (Enhanced Vegetation Index (EVI), Land Surface Water Index (LSWI)). We used multi-year (1998–2001) images from the VEGETATION sensor onboard the SPOT-4 satellite and CO<sub>2</sub> flux data from a CO<sub>2</sub> eddy flux tower site in Howland, Maine, USA. The seasonal dynamics of GPP predicted by the VPM model agreed well with observed GPP in 1998–2001 at the Howland Forest. These results demonstrate the potential of the satellite-driven VPM model for scaling-up GPP of forests at the CO<sub>2</sub> flux tower sites, a key component for the study of the carbon cycle at regional and global scales. © 2003 Elsevier Inc. All rights reserved.

**Keywords:** VEGETATION sensor; Vegetation index; Gross ecosystem exchange of CO<sub>2</sub>; Howland forest

### 1. Introduction

The boreal forest is the largest terrestrial biome on Earth and is composed of a small number of plant species. Although relatively simple in vegetation structure, boreal forests play an important role in the global cycles of carbon, water and nutrients as well as the climate system. Estimates of net primary productivity of boreal forests vary widely (Melillo et al., 1993; Schulze et al., 1999). In recent years, a number of field studies have used eddy covariance techniques to provide information on seasonal dynamics and interannual variation of net ecosystem exchange (NEE), ecosystem respiration (*R*) and gross primary production (GPP) of evergreen needleleaf forests across the world (Goulden et al., 1997; Hollinger et

al., 1999; Law et al., 2000, 2002; Schulze et al., 1999). Evergreen needleleaf forests can act as carbon sinks or carbon sources, depending upon climate and land use history. CO<sub>2</sub> flux data collected at flux tower sites provide invaluable information on ecosystem processes, and can be used to improve process-based ecosystem models (Law et al., 2000). Eddy flux towers at forest sites provide integrated flux measurements over large footprints that range from a few to many hectares, depending upon tower height and weather conditions. To scale-up CO<sub>2</sub> fluxes from flux tower sites is an important challenge in the study of the carbon cycle at regional and global scales.

Satellite remote sensing provides consistent and systematic observations of vegetation and ecosystems, and has played an increasing role in characterization of vegetation structure and estimation of gross primary production (GPP) or net primary production (NPP) of forests (Behrenfeld et al., 2001; Field et al., 1995, 1998; Potter et al., 1993; Prince & Goward, 1995; Ruimy et al., 1994, 1999; Running et al.,

\* Corresponding author. Tel.: +1-603-862-3818; fax: +1-603-862-0188.

E-mail address: [xiangming.xiao@unh.edu](mailto:xiangming.xiao@unh.edu) (X. Xiao).

1999, 2000). These satellite-based studies have used the light-use efficiency (LUE) approach to estimate either GPP (Prince & Goward, 1995; Running et al., 1999, 2000) or NPP (Field et al., 1995; Potter et al., 1993), and the formulations of these Production Efficiency Models (PEMs) are the following:

$$\text{GPP} = \epsilon_g \times \text{FAPAR} \times \text{PAR} \quad (1)$$

$$\text{NPP} = \epsilon_n \times \text{FAPAR} \times \text{PAR} \quad (2)$$

where PAR is the incident photosynthetically active radiation ( $\text{MJ m}^{-2}$ ) in a time period (day, month), FAPAR is the fraction of PAR absorbed by vegetation canopy, and  $\epsilon_g$  is the light use efficiency (LUE,  $\text{g C MJ}^{-1} \text{ PAR}$ ) in GPP calculation, and  $\epsilon_n$  is the light use efficiency in NPP calculation. The time step of the PEM models ranges from daily (Running et al., 2000) to monthly (Field et al., 1995), dependent upon image composites of the satellite.  $\epsilon_g$  or  $\epsilon_n$  is usually estimated as a function of temperature, soil moisture and/or water vapor pressure deficit (Field et al., 1995; Prince & Goward, 1995; Running et al., 2000).

FAPAR is closely related to Normalized Difference Vegetation Index (NDVI), which is calculated as a normalized ratio between red ( $\rho_{\text{red}}$ ) and near infrared ( $\rho_{\text{nir}}$ ) bands (Tucker, 1979):

$$\text{NDVI} = \frac{\rho_{\text{nir}} - \rho_{\text{red}}}{\rho_{\text{nir}} + \rho_{\text{red}}} \quad (3)$$

In remote sensing analysis, FAPAR is usually estimated as a linear or nonlinear function of NDVI (Prince & Goward, 1995; Ruimy et al., 1994; Running et al., 2000):

$$\text{FAPAR} = a + b \times \text{NDVI} \quad (4)$$

where the coefficients  $a$  and  $b$  vary, dependent upon the NDVI data set used by the PEM models (Prince & Goward, 1995). FAPAR is also closely related to leaf area index (LAI). A number of process-based global NPP models do not explicitly calculate FAPAR, but compute a leaf area index (Ruimy et al., 1999). FAPAR can be estimated as a function of LAI and light extinction coefficient ( $k$ ) (Ruimy et al., 1999):

$$\text{FAPAR} = 0.95(1 - e^{-k \times \text{LAI}}) \quad (5)$$

These PEM models are largely based on the quantitative LAI–FAPAR and NDVI–FAPAR relationships, and have been applied at regional to global scales, using monthly NDVI data from AVHRR sensors (Field et al., 1995; Potter et al., 1993; Prince & Goward, 1995) and SeaWiFS sensor (Behrenfeld et al., 2001). It is known that NDVI suffers several limitations, including sensitivity to atmospheric conditions, sensitivity to soil background, and saturation of NDVI values in multi-layered and closed canopies. In

addition, at the canopy level, vegetation canopies are composed of photosynthetically active vegetation (PAV, mostly green leaves) and non-photosynthetically active vegetation (NPV, mostly senescent foliage, branches and stems). NPV has a significant effect on FAPAR at the canopy level. For example, in forests with a leaf area index of  $< 3.0$ , NPV (stem surface) increased canopy FAPAR by 10–40% (Asner et al., 1998). At the leaf level, individual green leaves also have some proportion of NPV (e.g., primary/secondary/tertiary veins), dependent upon leaf age and type. Thus, FAPAR by a forest canopy must be partitioned into two components:

$$\text{FAPAR} = \text{FAPAR}_{\text{PAV}} + \text{FAPAR}_{\text{NPV}} \quad (6)$$

Only the PAR absorbed by PAV (i.e.,  $\text{FAPAR}_{\text{PAV}}$ ) is used for photosynthesis, therefore, any model that takes the conceptual partition of PAV and NPV of forest canopy into consideration is likely to improve estimation of the amount of PAR absorbed by the forest canopy (PAV) for photosynthesis and quantification of light use efficiency ( $\epsilon_g$  or  $\epsilon_n$ ) of vegetation over time.

A new generation of advanced optical sensors has recently come into operation, for instance, the VEGETATION (VGT) sensor onboard the SPOT-4 satellite (launched in March 1998) and the Moderate Resolution Imaging Spectroradiometer (MODIS) sensor onboard the Terra satellite (launched in December 1999). These new sensors have more spectral bands, in comparison to the AVHRR sensor that has only red and near infrared bands for vegetation study (calculation of NDVI). The VGT sensor onboard the SPOT-4 satellite has four spectral bands: blue (0.43–0.47  $\mu\text{m}$ ), red (0.61–0.68  $\mu\text{m}$ ), near infrared (NIR, 0.78–0.89  $\mu\text{m}$ ) and shortwave infrared (SWIR, 1.58–1.75  $\mu\text{m}$ ). Data availability of these spectral bands offers an opportunity to develop improved vegetation indices and incorporate them into new satellite-based models for improving estimation of GPP of vegetation at regional to global scales.

In this study, our objective is to develop and validate a new satellite-based Vegetation Photosynthesis Model (VPM) that estimates GPP of evergreen needleleaf forests over the plant-growing season, using the improved vegetation indices that can be derived from the new generation of advanced optical sensors (e.g., VGT). Our approach is to combine the multi-year (1998–2001) image data from the VGT sensor onboard the SPOT-4 satellite with  $\text{CO}_2$  flux data from an eddy flux tower site at Howland, Maine, USA. The  $\text{CO}_2$  eddy flux tower site is located near Howland, Maine (45.20407°N and 68.74020°W, 60-m elevation). The vegetation of this 90-year-old evergreen needleleaf forest is about 41% red spruce (*Pinus rubens* Sarg), 25% eastern hemlock (*Tsuga canadensis* (L.) Carr.), 23% other conifers and 11% hardwoods (Hollinger et al., 1999). The leaf area index (LAI) of the forest stand is about 5.3  $\text{m}^2/\text{m}^2$ . Plant-growing season usually starts around mid-April ( $\sim$  day

100) and lasts about 180 days. Eddy flux measurements of CO<sub>2</sub>, H<sub>2</sub>O and energy at the site have been conducted since 1996 (Hollinger et al., 1999) and is part of the AmeriFlux network (<http://public.ornl.gov/ameriflux/Data/index.cfm>). Availability of CO<sub>2</sub> flux data from a CO<sub>2</sub> flux tower site of evergreen needleleaf forest makes it possible (1) to evaluate the relationship between the improved vegetation indices and photosynthetic activities of vegetation, and (2) to assess satellite-based models that estimate the seasonal dynamics of GPP of forests at the spatial and temporal scales that are relatively consistent between satellite observations and flux tower measurements. Any improvement in representation of seasonal dynamics of GPP of forests by the satellite-based models will enrich our understanding of net CO<sub>2</sub> exchange between the forest ecosystems and the atmosphere over time. This study is one of many steps towards our long-term goal for development and application of the satellite-based VPM model to quantify the spatial patterns and temporal dynamics of GPP of evergreen boreal forests across the globe at 1-km spatial resolution.

## 2. A brief description of vegetation indices

A number of vegetation indices have been developed for broad-waveband optical sensors (e.g., Landsat, AVHRR) over the last few decades, and can be generalized into three categories: (1) vegetation indices that use only red and NIR spectral bands, including NDVI; (2) vegetation indices that use blue, red and NIR spectral bands; and (3) vegetation indices that use NIR and SWIR spectral bands. Here we briefly review the last two categories of vegetation indices.

### 2.1. Vegetation indices that use blue, red and NIR bands

The blue band is primarily used for atmospheric correction, and has also been used in developing improved vegetation indices that use blue, red and near infrared bands. For instance, to account for residual atmospheric contamination (e.g., aerosols) and variable soil background reflectance, the Enhanced Vegetation Index (EVI) was developed (Huete et al., 1997, 2002; Justice et al., 1998). EVI directly normalizes the reflectance in the red band as a function of the reflectance in the blue band (Huete et al., 1997):

$$EVI = G \times \frac{\rho_{nir} - \rho_{red}}{\rho_{nir} + (C_1 \times \rho_{red} - C_2 \times \rho_{blue}) + L} \quad (7)$$

where  $G=2.5$ ,  $C_1=6$ ,  $C_2=7.5$ , and  $L=1$  (Huete et al., 1997).

EVI is linearly correlated with the green leaf area index (LAI) in crop fields, based on airborne multispectral data (Boegh et al., 2002). Evaluation of radiometric and biophysical performance of EVI calculated from the Moderate Resolution Imaging Spectroradiometer (MODIS) sensor indicated that EVI remained sensitive to canopy variations

(Huete et al., 2002). In an earlier study that compared VGT-derived NDVI and EVI for Northern Asia over the period of 1998–2001, the results indicated that EVI is less sensitive to residual atmospheric contamination due to aerosols from extensive fires in 1998 (Xiao et al., 2003).

Significant effort and progress have been made in developing advanced vegetation indices that are optimized for retrieval of FAPAR from individual optical sensors (Gobron et al., 1999, 2000; Govaerts et al., 1999). Detailed information on mathematical formulae and parameters of these vegetation indices was given elsewhere (Gobron et al., 2000). The implementation of these vegetation indices requires the top-of-atmosphere (TOA) bidirectional reflectance factors (BRFs) data as input data, and blue band is used to rectify red and NIR bands (Gobron et al., 2000). These vegetation indices have been optimized for the Medium Resolution Imaging Spectrometer (MERIS), the Global Imager (GLI) and the VEGETATION sensors.

### 2.2. Vegetation indices that use NIR and SWIR bands

In comparison to numerous studies that use red and NIR spectral bands (e.g., in calculation of NDVI), a limited number of studies have explored the SWIR spectral bands (e.g., 1.6 and 2.1  $\mu\text{m}$ ) for vegetation study. It was reported that the SWIR band (1.6  $\mu\text{m}$ ) was sensitive to plant water content (Tucker, 1980). In order to calculate leaf water content, field and laboratory work are needed to measure fresh weight (FW) and dry weight (DW) as well as specific leaf area (SLA,  $\text{cm}^2/\text{g}$ ) of leaves. Leaf water content is usually described by (1) foliage moisture content (FMC, %, calculated as  $(FW - DW) \times 100/FW$ , or  $(FW - DW) \times 100/DW$ ) and (2) equivalent water thickness (EWT,  $\text{g}/\text{cm}^2$ , calculated as  $(FW - DW)/\text{Leaf Area}$ ). A number of studies have suggested that a combination of NIR and SWIR bands have the potential for retrieving leaf and canopy water content (EWT,  $\text{g}/\text{cm}^2$ ), based on Landsat image data (Hunt & Rock, 1989), hyperspectral image data (Gao, 1996; Serrano et al., 2000b) and VGT data (Ceccato et al., 2001, 2002a,b). The Moisture Stress Index (MSI), which is calculated as a simple ratio between SWIR (1.6  $\mu\text{m}$ ) and NIR (0.82  $\mu\text{m}$ ) spectral bands, was proposed to estimate leaf relative water content (%) and equivalent water thickness (EWT,  $\text{g}/\text{cm}^2$ ) of different plant species (Hunt & Rock, 1989):

$$MSI = \frac{\rho_{swir}}{\rho_{nir}} \quad (8)$$

The above MSI index (a simple ratio between SWIR and NIR bands) could be used as a first approximation to retrieve equivalent water thickness ( $\text{g}/\text{cm}^2$ ) at leaf level, based on laboratory measurements, the radiative transfer model (PROSPECT) and a sensitivity analysis (Ceccato et al., 2001). In analyses of the 10-day composite of VGT data that are freely available to users through the website (<http://>

free.vgt.vito.be), another water index was calculated as the normalized difference between the NIR (0.78–0.89  $\mu\text{m}$ ) and SWIR (1.58–1.75  $\mu\text{m}$ ) spectral bands (Xiao et al., 2002c), here it is called “Land Surface Water Index (LSWI)”:

$$\text{LSWI} = \frac{\rho_{\text{nir}} - \rho_{\text{swir}}}{\rho_{\text{nir}} + \rho_{\text{swir}}} \quad (9)$$

Analyses of multi-temporal VGT data have shown that LSWI is useful for improving classification of cropland and forests (Xiao et al., 2002a,b,c). This water index is similar in mathematic formulation to the Normalized Difference Water Index (NDWI) that uses reflectance values in the 0.86 and 1.24  $\mu\text{m}$  spectral bands of hyperspectral data (Gao, 1996):

$$\text{NDWI} = \frac{\rho_{0.86} - \rho_{1.24}}{\rho_{0.86} + \rho_{1.24}} \quad (10)$$

Recently, Ceccato et al. (2002a,b) proposed the Global Vegetation Moisture Index (GVMI) to retrieve equivalent water thickness ( $\text{g}/\text{m}^2$ ) at canopy level, using images from the VGT sensor:

$$\text{GVMI} = \frac{(\rho_{\text{nir}(\text{rectified})} + 0.1) - (\rho_{\text{swir}} + 0.02)}{(\rho_{\text{nir}(\text{rectified})} + 0.1) + (\rho_{\text{swir}} + 0.02)} \quad (11)$$

where  $\rho_{\text{nir}(\text{rectified})}$  is the reflectance values of the rectified NIR band, which are derived from a complex procedure that involves blue spectral band and uses the apparent reflectance as seen at the top-of-atmosphere (VGT-P product, <http://www.vgt.vito.be>) as input data (Gobron et al., 2000). Field data collected at shrub steppe, shrub savannah, tree savannah and woodland in Senegal (West Africa) during 1998–2000 were used to evaluate the potential of GVMI for retrieval of EWT at canopy level (Ceccato et al., 2002a). The comparison between GVMI and NDVI shows that GVMI provides information related to canopy water content (EWT), while NDVI provides information related to vegetation greenness (Ceccato et al., 2002a).

### 3. Description of the satellite-based Vegetation Photosynthesis Model (VPM)

#### 3.1. Overview of the VPM model

Based on the conceptual partition of NPV and PAV within a canopy (see Eq. (6)), we proposed a new satellite-based Vegetation Photosynthesis Model (VPM) for estimation of GPP over the photosynthetically active period of vegetation (Fig. 1):

$$\text{GPP} = \varepsilon_g \times \text{FAPAR}_{\text{PAV}} \times \text{PAR} \quad (12)$$

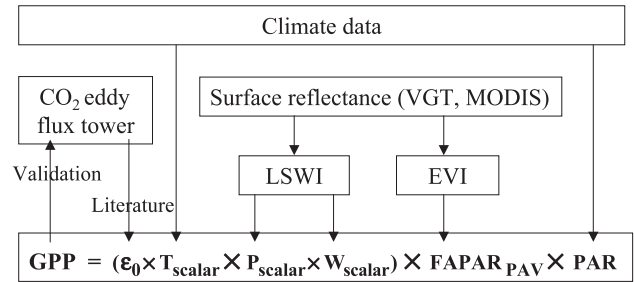


Fig. 1. The schematic diagram of the Vegetation Photosynthesis Model (VPM). EVI—Enhanced Vegetation Index; LSWI—Land Surface Water Index;  $\text{FAPAR}_{\text{PAV}}$ —the fraction of photosynthetically active radiation (PAR) absorbed by the photosynthetic active vegetation (PAV) in the canopy;  $T_{\text{scalar}}$ ,  $P_{\text{scalar}}$  and  $W_{\text{scalar}}$ —scalars for temperature, leaf phenology and canopy water content, respectively; GPP—gross primary production of terrestrial ecosystems;  $\varepsilon_0$ —maximum light use efficiency ( $\mu\text{mol CO}_2/\mu\text{mol PPF}$ ). VGT—VEGETATION sensor onboard the SPOT-4 satellite; MODIS—Moderate Resolution Imaging Spectroradiometer onboard the NASA Terra and Aqua satellites.

where PAR is the photosynthetically active radiation ( $\mu\text{mol}$  photosynthetic photon flux density, PPF), and  $\varepsilon$  is the light use efficiency ( $\mu\text{mol CO}_2/\mu\text{mol PPF}$ ). Light use efficiency ( $\varepsilon$ ) is affected by temperature, water, and leaf phenology:

$$\varepsilon_g = \varepsilon_0 \times T_{\text{scalar}} \times W_{\text{scalar}} \times P_{\text{scalar}} \quad (13)$$

where  $\varepsilon_0$  is the apparent quantum yield or maximum light use efficiency ( $\mu\text{mol CO}_2/\mu\text{mol PPF}$ ), and  $T_{\text{scalar}}$ ,  $W_{\text{scalar}}$  and  $P_{\text{scalar}}$  are the scalars for the effects of temperature, water and leaf phenology on light use efficiency of vegetation, respectively.

$T_{\text{scalar}}$  is estimated at each time step, using the equation developed for the Terrestrial Ecosystem Model (Raich et al., 1991):

$$T_{\text{scalar}} = \frac{(T - T_{\text{min}})(T - T_{\text{max}})}{[(T - T_{\text{min}})(T - T_{\text{max}})] - (T - T_{\text{opt}})^2} \quad (14)$$

where  $T_{\text{min}}$ ,  $T_{\text{max}}$  and  $T_{\text{opt}}$  are minimum, maximum and optimal temperature for photosynthetic activities, respectively. If air temperature falls below  $T_{\text{min}}$ ,  $T_{\text{scalar}}$  is set to be zero.

The effect of water on plant photosynthesis ( $W_{\text{scalar}}$ ) has been estimated as a function of soil moisture and/or water vapor pressure deficit (VPD) in a number of PEM models (Field et al., 1995; Prince & Goward, 1995; Running et al., 2000). For instance, in the CASA (Carnegie, Stanford, Ames Approach) model, soil moisture was estimated using a one-layer bucket model (Malmstrom et al., 1997). Soil moisture represents water supply to the leaves and canopy, and water vapor pressure deficit represents evaporative demand in the atmosphere. Leaf and canopy water content is largely determined by dynamic changes of both soil moisture and water vapor pressure deficit. As the first order of approximation, here we proposed an alternative and

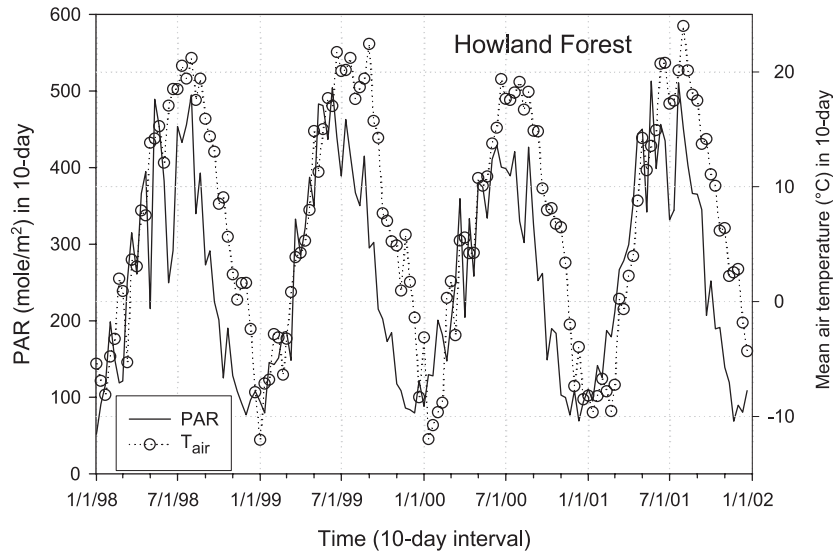


Fig. 2. The seasonal dynamics of photosynthetically active radiation (PAR) and mean air temperature during 1998–2001 at the eddy flux tower site of Howland Forest, Maine, USA.

simple approach that uses a satellite-derived water index (see Eq. (9)) to estimate the seasonal dynamics of  $W_{\text{scalar}}$

$$W_{\text{scalar}} = \frac{1 + \text{LSWI}}{1 + \text{LSWI}_{\text{max}}} \quad (15)$$

where  $\text{LSWI}_{\text{max}}$  is the maximum LSWI within the plant-growing season for individual pixels. When multi-year LSWI data are available, we will calculate the mean LSWI values of individual pixels over multiple years at individual temporal points (daily, weekly or 10-day), and then select the maximum LSWI value within the photosynthetically active period as an estimate of  $\text{LSWI}_{\text{max}}$ .

In the VPM model,  $P_{\text{scalar}}$  is included to account for the effect of leaf age on photosynthesis at canopy level. Leaf age affects the seasonal patterns of photosynthetic capacity and net ecosystem exchange of carbon in a deciduous forest (Wilson et al., 2001). In comparing daily light use efficiency from four  $\text{CO}_2$  flux tower sites (an agriculture field, a tallgrass prairie, a deciduous forest and a boreal forest), the results support inclusion of parameters for cloudiness and the phenological status of the vegetation (Turner et al., 2003). In the VPM model, calculation of  $P_{\text{scalar}}$  is dependent upon life expectancy of leaves (deciduous versus evergreen). For a canopy that is dominated by leaves with a life expectancy of 1 year (one growing season, e.g., deciduous trees),  $P_{\text{scalar}}$  is calculated at two different phases (note that detailed discussion of  $P_{\text{scalar}}$  of deciduous forests will be presented in another paper.):

$$P_{\text{scalar}} = \frac{1 + \text{LSWI}}{2} \quad (16)$$

During bud burst to leaf full expansion

$$P_{\text{scalar}} = 1 \quad \text{After leaf full expansion} \quad (17)$$

Evergreen needleleaf trees in temperate and boreal zones have a green canopy throughout the year, because foliage is retained for several growing seasons. Canopy of evergreen needleleaf forests is thus composed of green leaves at various ages. Fixed turnover rates of foliage of evergreen needleleaf forests at canopy level were used in some process-based ecosystem models (Aber & Federer, 1992; Law et al., 2000). In this version of the VPM model, therefore, a simple assumption of  $P_{\text{scalar}}$  is made for evergreen needleleaf forests:

$$P_{\text{scalar}} = 1 \quad (18)$$

Photosynthetic activity of vegetation canopy is in part determined by the amount of PAR the PAV absorbs for photosynthesis. To accurately estimate  $\text{FAPAR}_{\text{PAV}}$  in forests is a challenge to both radiative transfer modeling and field measurements. In this version of the VPM model,  $\text{FAPAR}_{\text{PAV}}$  within the photosynthetically active period of vegetation is estimated as a linear function of EVI:

$$\text{FAPAR}_{\text{PAV}} = \text{EVI} \quad (19)$$

### 3.2. Estimation of model parameters for evergreen boreal forests

The  $\varepsilon_0$  values vary with vegetation types, and information about  $\varepsilon_0$  for individual vegetation types can be obtained from a survey of the literature (Ruimy et al., 1995) and/or analysis of gross ecosystem exchange of  $\text{CO}_2$  and photosynthetic photon flux density (PPFD) at a  $\text{CO}_2$  eddy flux tower site (Goulden et al., 1997). Estimation of the  $\varepsilon_0$  parameter is largely determined by the choice of either a linear or nonlinear model (e.g., hyperbolic equation) between GPP and incident PPFD data (generally at half-hour

time-step) over a year (Frolking et al., 1998; Ruimy et al., 1995, 1996):

$$NEE = \beta \times PPFD - R \tag{20}$$

$$NEE = \frac{\alpha \times PPFD \times GEE_{max}}{\alpha \times PPFD + GEE_{max}} - R \tag{21}$$

where  $\alpha$  is apparent quantum yield (as PPFD approaches to 0), and  $\beta$  is the slope of the linear fit.

For instance, in a review study that examined the relationship between GPP and PPFD from 126 published data

sets (Ruimy et al., 1995), it was reported that in a linear model,  $GPP = 0.020 \times PPFD$  (i.e.,  $\epsilon_0 = 0.020 \mu\text{mol CO}_2/\mu\text{mol PPFD}$  or  $\sim 0.24 \text{ g C/mol PPFD}$ ), but in a nonlinear hyperbolic function,  $GPP = 0.044 \times PPFD \times 43.35 / (0.044 \times PPFD + 43.35)$  (i.e.,  $\epsilon_0 = 0.044 \mu\text{mol CO}_2/\mu\text{mol PPFD}$  or  $\sim 0.528 \text{ g C/mol PPFD}$ ). In the VPM model,  $\epsilon_0$  values derived from the hyperbolic function are used.

In order to obtain  $\epsilon_0$  value for the VPM model, a literature survey was conducted to gather published information on  $\epsilon_0$  for evergreen needleleaf forests, in those publications  $\epsilon_0$  values were estimated using the nonlinear hyperbolic function (Eq. (21)). The Boreal Ecosystem–Atmosphere Study (BOREAS) conducted  $\text{CO}_2$  flux mea-

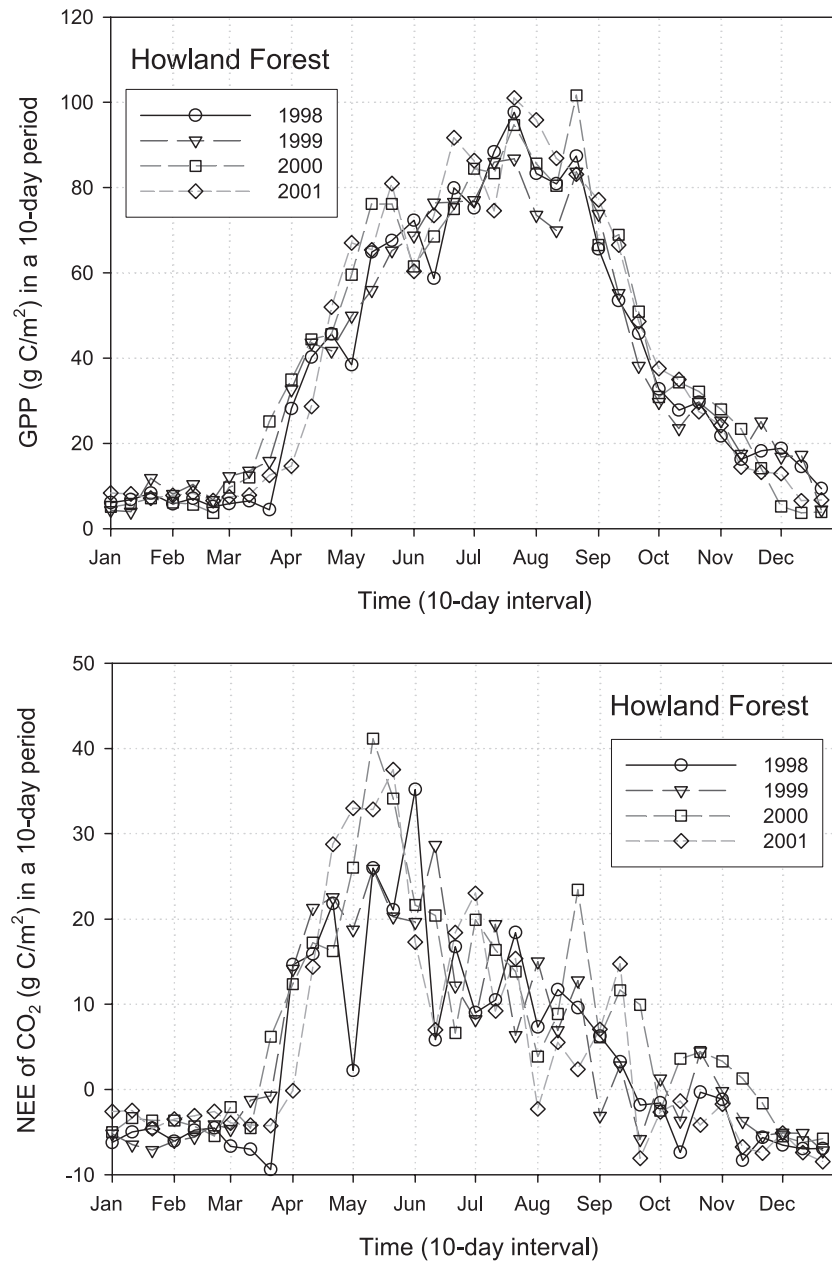


Fig. 3. The seasonal dynamics of net ecosystem exchange of  $\text{CO}_2$  (NEE) and gross primary production (GPP) at the eddy flux tower of Howland Forest, Maine, USA.

surement at a few evergreen needleleaf forest sites in Canada. During 3/16/1994–10/31/1996, the eddy covariance technique was used to measure net ecosystem exchange of  $\text{CO}_2$  between the atmosphere and a black spruce (*Picea mariana*) forest in central Manitoba, Canada (Goulden et al., 1997). The site (55.879°N, 98.484°W) is dominated by 10-m-tall 120-year-old black spruce, with a minor layer of shrubs and continuous feather moss. Through examination of the relationship between GPP and incident photosynthetically active photon flux density (PPFD), it was reported that apparent quantum yield for the tower site is  $\epsilon_0 = 0.040 \mu\text{mol CO}_2/\mu\text{mol PPFD}$  (Goulden et al., 1997). Similarly, an intensive field campaign (IFC) was conducted in midsummer or peak growing season (IFC-2 = July 26 to August 8, 1994) at the *P. mariana* forest (old black spruce, or OBS site, located at 53.85°N and 105.12°W) in Canada (Sullivan et al., 1997). Vegetation at the site consists primarily of a *P. mariana* overstory (up to 12 m tall and 155 years of age) with some tamarack and *Pinus banksiana* present. The apparent quantum yields calculated from the data measured in IFC-2 were  $0.041 \pm 0.003$  for upper canopy and  $0.035 \pm 0.002$  ( $\mu\text{mol CO}_2/\mu\text{mol PPFD}$ ) for lower canopy, respectively (Sullivan et al., 1997). In this study, we used  $\epsilon_0 = 0.040 \mu\text{mol CO}_2/\mu\text{mol PPFD}$ , or 0.48 g C/mole PAR for evergreen needleleaf forest (Goulden et al., 1997). The  $\epsilon_0 = 0.040 \mu\text{mol CO}_2/\mu\text{mol PPFD}$  value was also used in the 3-PG model that uses leaf area index to calculate FAPAR of a *Pinus ponderosa* forest (Law et al., 2000). In the standard MODIS-based GPP/NPP algorithm (MOD17) that uses NDVI to calculate FAPAR (Running et al., 1999, 2000), the  $\epsilon_0$  value of evergreen needleleaf forest is 1.008 g C/MJ (approximately 0.46–0.49 g C/mol PPFD), very close

to the 0.48 g C/mol PPFD used here from a boreal forest tower site in Canada (Goulden et al., 1997), based on an approximate conversion of 2.05–2.17 between MJ ( $10^6$  J) and mol PPFD (Aber et al., 1996; Weiss & Norman, 1985).

In calculation of  $T_{\text{scalar}}$  (see Eq. (14)),  $T_{\text{min}}$ ,  $T_{\text{opt}}$  and  $T_{\text{max}}$  values vary among different vegetation types (Aber & Federer, 1992; Raich et al., 1991). For evergreen needleleaf forest, we use 0, 20 and 40 °C for  $T_{\text{min}}$ ,  $T_{\text{opt}}$  and  $T_{\text{max}}$ , respectively (Aber & Federer, 1992). Photosynthesis of conifers in temperate to boreal zones is limited by low temperatures (DeLucia & Smith, 1987). To better capture the effect of air temperature, in calculation of  $T_{\text{scalar}}$ , instead of using the daily mean air temperature that is calculated as the average value between daily maximum temperature (generally daytime) and daily minimum temperature (night time), we used the average daytime temperature, which was calculated as the average between daily mean temperature and daily maximum temperature (Aber & Federer, 1992).

#### 4. Site-specific data for simulation and validation of the VPM model

##### 4.1. Description of site-specific field data

Daily climate (maximum/minimum temperature, precipitation) and photosynthetically active radiation (mol/day PPFD) data during 1996–2001 at Howland Forest were available for this study. The annual mean air temperature during 1996–2001 was about 6.7 °C, while the annual mean daytime air temperature during 1996–2001 was about 9.2 °C. In order to be consistent with the 10-day composite

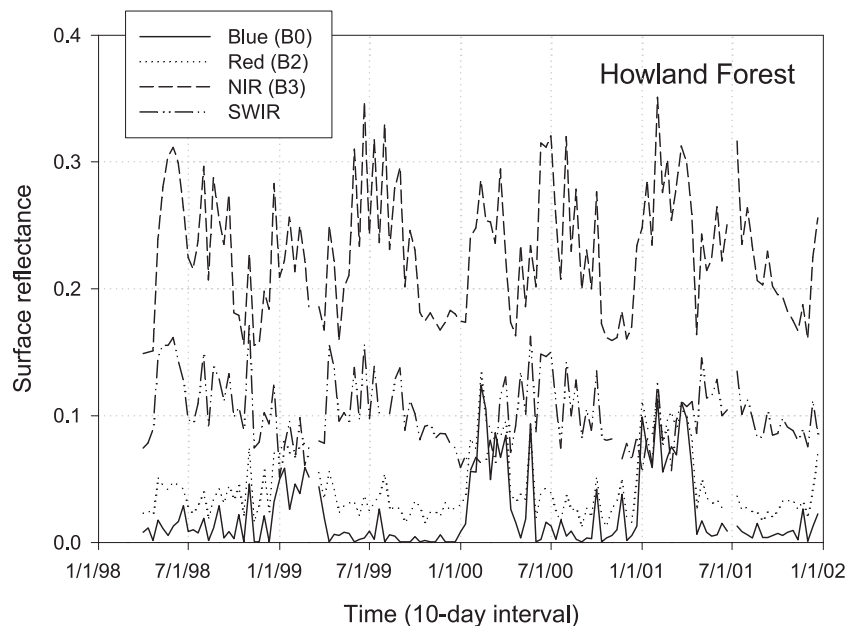


Fig. 4. The seasonal dynamics of surface reflectance values of four spectral bands of VEGETATION sensor during 1998–2001 at the eddy flux tower site of Howland Forest, Maine, USA.

satellite images we used (see Section 3.2), we calculated the 10-day mean temperature from the daily temperature data, and the 10-day sum of PAR from the daily PAR data, respectively (Fig. 2).

Daily flux data of NEE, GPP and ecosystem respiration ( $R$ ) at Howland Forest during 1996–2001 were generated from the half-hourly flux data. Half-hourly values were calculated from the covariance of the fluctuations in vertical wind speed and  $\text{CO}_2$  concentration measured at 5 Hz (Hollinger et al., 1999). Half-hourly flux values were excluded from further analysis if the wind speed was below  $0.5 \text{ m s}^{-1}$ , sensor variance was excessive, rain or snow was falling, for incomplete half-hour sample periods, or instrument malfunction. At night flux values were excluded from further analysis if the friction velocity ( $u^*$ ) was below a threshold of 0.25. To obtain annual estimates of  $\text{CO}_2$  exchange, values missing from the half-hourly record of annual NEE were modeled by combining estimates of canopy photosynthesis and nocturnal respiration. Daytime  $\text{CO}_2$  exchange rates were obtained from Michaelis–Menten models of PPFD with coefficients fitted on a monthly basis. Missing nocturnal  $\text{CO}_2$  exchange values were obtained from second order Fourier regressions between Julian day and nocturnal respiration. Filled half-hourly NEE data were used to estimate respiration and GPP in the following way. All data points with PAR values less than  $5 \mu\text{mol m}^{-2} \text{ s}^{-1}$  were used to estimate dark respiration rate. For each year, all “dark” NEE values were regressed against measured soil temperature. The resulting regression equation was then used with measured soil temperatures to predict respiration during “light” periods ( $\text{PAR} > 5 \mu\text{mol m}^{-2} \text{ s}^{-1}$ ). GPP was then estimated as NEE minus estimated respiration for all “light” periods (using convention of opposite signs for GPP and respiration). We calculated the 10-day sums of GPP and NEE from the daily GPP and NEE data, in order to be consistent with the 10-day composite satellite images we used (Fig. 3).

#### 4.2. Description of images from the VEGETATION sensor

We used 10-day composite images from the VEGETATION (VGT) optical sensor onboard the SPOT-4 satellite that was launched in March 1998. The VGT sensor provides daily images for the globe at 1-km spatial resolution. Standard 10-day synthetic products (VGT-S10) are generated by selecting a pixel with the maximum Normalized Difference Vegetation Index (NDVI) value in a 10-day period, and are freely available to the public (<http://free.vgt.vito.be>). There are three 10-day composites within a month: days 1–10, 11–20, and 21 to the end of month. We acquired the VGT-S10 data over the period of April 1–10, 1998 to December 21–31, 2002 for the globe. Details on methods for pre-processing and calculation of vegetation indices from VGT-S10 data were presented elsewhere (Xiao et al., 2002c, 2003). In this study, we extracted spectral bands from one 1-km pixel that covers

the eddy flux tower site at Howland Forest (Fig. 4), based on the geographical information (latitude and longitude) of the tower, and then calculated vegetation indices (Fig. 5). In order to estimate  $\text{LSWI}_{\text{max}}$  for the Howland Forest site, we calculated the mean seasonal cycle of LSWI for all 10-day periods in the 4-year data set (1998–2001). The resulting mean seasonal data at the 10-day interval represents a

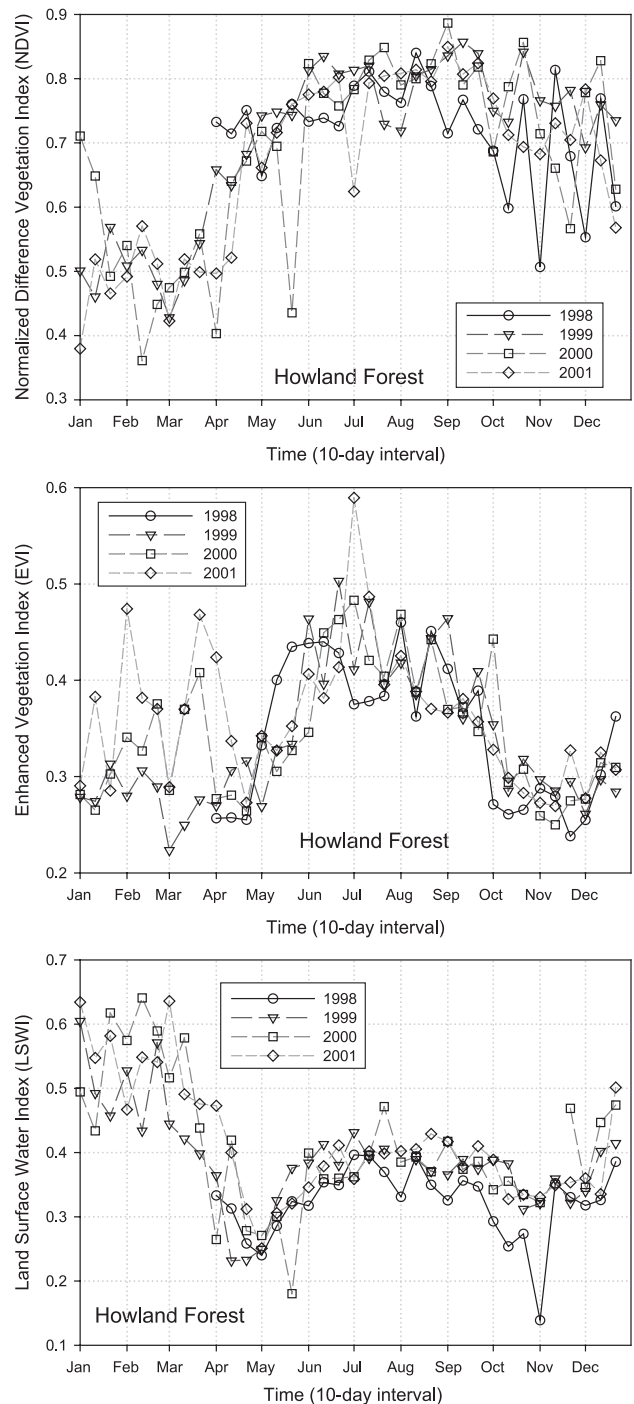


Fig. 5. The seasonal dynamics of vegetation indices during 1998–2001 at the eddy flux tower site of Howland Forest, Maine, USA.

“typical year”, and we then selected the maximum LSWI value (0.41; July 21–31) within April 1–November 10 as an estimate of  $LSWI_{max}$  (i.e.,  $LSWI_{max} = 0.41$ ).

### 5. Results

#### 5.1. Seasonal dynamics of EVI and NDVI for evergreen needleleaf forest

The seasonal dynamics of EVI differs from that of NDVI during late April–early November in terms of both magnitude and phase (Fig. 5). During summer (June, July and August) of 1998–2001, the maximum NDVI value ranges in the order of 0.80–0.85, and were much higher than the maximum EVI values (in the order of ~ 0.5). When calculating FAPAR using LAI for the Howland Forest site (see Eq. (5), with  $k=0.5$ ,  $LAI=5.3 \text{ m}^2/\text{m}^2$ ), the resultant FAPAR is about 0.88. There were relatively large differences between NDVI and EVI over the plant-growing season at 10-day interval in 1998–2001 (Figs. 5 and 6).

During the plant-growing season, EVI reached its peak in early summer and then declined gradually (Figs. 5 and 6). The observed decrease of EVI after reaching its peak in early summer may be caused by many factors, including complex interactions between atmosphere and leaf/canopy as well as leaf optical property. In addition to the correction term ( $6 \times \rho_{red} - 7.5 \times \rho_{blue}$ ) in the EVI equation, which corrects residual atmospheric contamination above the canopy, changes in leaf properties may also contribute to the decline of EVI over time. Evergreen needleleaf trees consist of leaves with various ages of years. As a needleleaf gets old, it changes in its size (e.g., leaf thickness), dry weight, chlorophyll content and nitrogen content. Based on a comparative assessment of needle anatomy of red spruce (Rock et al., 1994), needleleaf thickness of 1st year leaves ( $726 \pm 44 \mu\text{m}$ ) is about 11% smaller than that of 2nd year leaves ( $803 \pm 46 \mu\text{m}$ ), and there is less intercellular air space (%) in the 2nd year leaves. Although chlorophyll and nitrogen concentrations (mg/g DW) may be relatively stable over seasons, an increase in leaf thickness results in a larger volume of needleleaf, which leads to dilution effect of chlorophyll and nitrogen in the needleleaf ( $\text{mg}/\text{cm}^3$ ). The changes in leaf size (e.g., thickness), intercellular air space, dry weight, and the dilution effect might together affect reflectance, transmittance and absorption of needleleaf, for instance, the 2nd year needles of red spruce have slightly higher reflectance values in blue band but little change of reflectance values in red band, in comparison to the first-year needles (Rock et al., 1994). The adjusting factor ( $L=1$ ) for soil and vegetation background in the correction term ( $6 \times \rho_{red} - 7.5 \times \rho_{blue} + L$ ) of EVI equation also plays a large role in the seasonal dynamics of EVI. After reaching its peak in early summer, NIR values declined gradually, resulting in lower EVI values (Fig. 4).

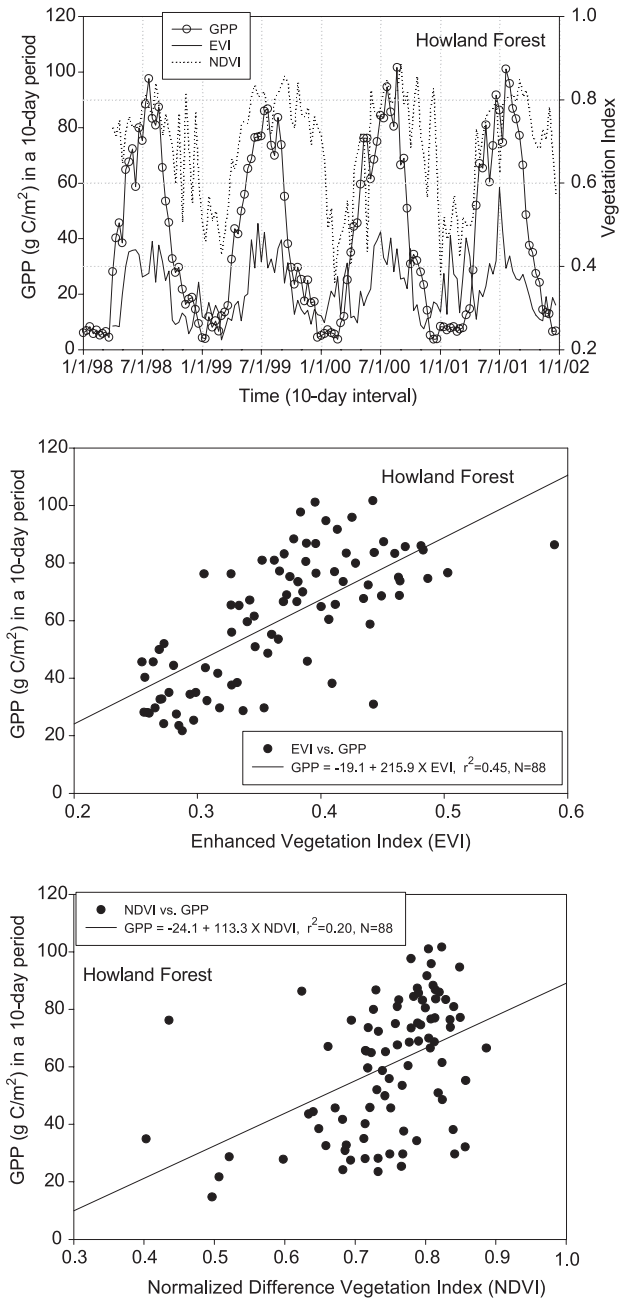


Fig. 6. A comparison between vegetation indices and gross primary production (GPP) at the eddy flux tower site of Howland Forest, Maine, USA. The data within the period of April 1 to November 10 during 1998–2001 were used. The simple linear regression models between GPP and EVI or NDVI have a  $P < 0.0001$ .

The comparisons between vegetation indices (EVI, NDVI) and GPP show that the seasonal dynamics of EVI followed those of GPP better than NDVI in terms of phase and amplitude of GPP (Fig. 6). When using all the observations within April 1 to November 10 during 1998–2001, EVI has a stronger linear relationship with GPP than NDVI (Fig. 6). The NDVI curve seems to be out of phase with GPP in the early and late part of the plant-growing season. After its peak in early summer, EVI gradually declined over

Table 1

Time-integrated sums of gross primary production ( $\text{g C/m}^2$ , GPP), photosynthetically active radiation ( $\text{mol/m}^2$ , PAR), and precipitation (mm, PPT) at Howland Forest, Maine, USA

Year	Tower data		VPM model	PAR and climate	
	GPP <sub>obs</sub> (1–12)	GPP <sub>obs</sub> (4–11)	GPP <sub>pred</sub> (4–11)	PAR <sub>4–11</sub>	PPT <sub>4–11</sub>
1998	1418	1285	1171	7108	586
1999	1430	1262	1227	7578	591
2000	1514	1384	1102	6858	527
2001	1506	1379	1253	7786	393

GPP<sub>obs</sub> (1–12) is the observed GPP from January to December. GPP<sub>obs</sub> (4–11), GPP<sub>pred</sub> (4–11), PAR<sub>4–11</sub> and PPT<sub>4–11</sub> are the observed GPP, predicted GPP, PAR and PPT over the period of April 1 to November 10, respectively.

late summer and fall seasons while NDVI had little change during the same period (Fig. 6).

### 5.2. Seasonal dynamics of LSWI for evergreen needleleaf forest

Among the three vegetation indices (LSWI, EVI, and NDVI), the seasonal dynamics LSWI is unique and characterized by a “spring trough” and a “fall trough” (Fig. 5). At Howland Forest site, forest stands in the winter and early spring is largely composed of snow, wet soil and vegetation. A snow pack of up to 2 m could exist from December to March. Snow has much higher reflectance in visible and near infrared bands, in comparison to vegetation. The high LSWI values in winter and early spring are attributed to snow cover in the forest stands. As snow melted in late spring, LSWI declined. The 10-day periods that had minimum LSWI in spring season were May 1–10 (1998), April 11–20 (1999), April 1–10 (2000) and May 1–10 (2001),

respectively. The “spring trough” corresponds to the beginning of photosynthetically active period of evergreen needleleaf forest. LSWI increased through spring and reached its peak in late July. The 10-day periods that have minimum LSWI in fall season were November 1–10 (1998), October 21–31 (1999), November 1–10 (2000) and October 11–20 (2001). The “fall trough” corresponds to the ending of photosynthetically active period. Seasonally integrated GPP over the period of April 1 to November 10 accounts for 91% (1998), 88% (1999), 91% (2000) and 92% (2001) of the annually integrated GPP from January 1 to December 31, respectively (Table 1). The “spring trough” and “fall trough” of LSWI time series within a year were also observed in an earlier study that examined multi-temporal LSWI data for deciduous broadleaf forests and evergreen needleleaf forests in Northeastern China (Xiao et al., 2002c).

LSWI time series data in 1998–2001 had distinct seasonal dynamics within the plant-growing season (Fig. 5). We also calculated the Moisture Stress Index (MSI, see Eq. (8)) for all 10-day composites of VGT data in 1998–2001 and the comparison between MSI and LSWI (Fig. 7) shows that there is a close relationship between MSI and LSWI for evergreen needleleaf forest at Howland Forest site. The results from a modeling study that used the PROSPECT radiative transfer model confirmed the relationship between equivalent water thickness (EWT,  $\text{g/cm}^2$ ) and the MSI, and MSI could therefore be used as a first approximation to retrieve vegetation water content at leaf level (Ceccato et al., 2001). At canopy level,  $\text{EWT}_{\text{canopy}}$  ( $\text{g/m}^2$ ) is a product of  $\text{EWT}_{\text{leaf}}$  ( $\text{g/m}^2$ ) and leaf area index (LAI,  $\text{m}^2/\text{m}^2$ ) (Ceccato et al., 2002b). No field measurements of leaf and canopy water content at Howland Forest site during 1998–2001

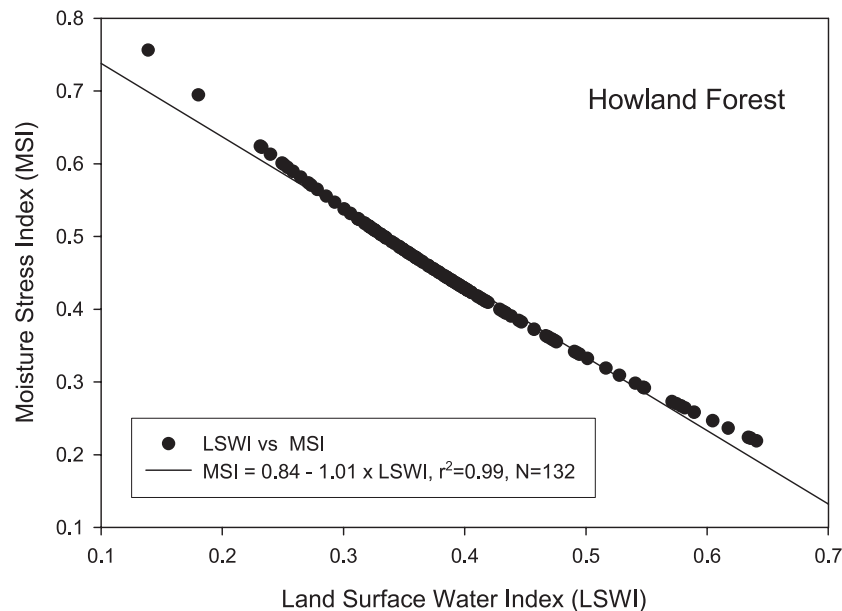


Fig. 7. A comparison between the Land Surface Water Index (LSWI) and Moisture Stress Index (MSI) during 1998–2001 at the eddy flux tower site of Howland Forest, Maine, USA.

were available for comparison between LSWI and vegetation water content. However, field sampling of fresh weight (FW) and dry weight (DW) of spruce and hemlock needles at Howland Forest site were conducted on six dates (5/19, 6/6, 7/9, 7/16, 8/7, 9/11) in 2002. Foliage moisture content (FMC, %) at Howland Forest was calculated using fresh weight (FW) and dry weight (DW) of leaves ( $=100 \times (FW - DW)/FW$ ). Because no field measurements of specific leaf weight (SLW,  $g/cm^2$ ) and leaf area index (LAI) were conducted on those sampling dates in 2002, we cannot accurately calculate EWT on those sampling dates. Unlike the grassland and savannah vegetation that have large seasonal changes in SLW and LAI over the plant-growing season (Ceccato et al., 2002a), mature stands of evergreen

needleleaf forests have only slightly changes in LAI and SLW over the plant-growing season, and therefore, single LAI and SLW values were often used in estimation of GPP of evergreen needleleaf forests by some process-based ecosystem models (Aber & Federer, 1992; Law et al., 2000). As a simple approximation, we used  $LAI = 5.3 m^2/m^2$  and  $SLW = 280 g/m^2$  (Aber & Federer, 1992) to estimate EWT of evergreen needleleaf forest for the six sampling dates at Howland site (Fig. 8), and the resultant EWT varied from  $0.018 g/cm^2$  (5/19/2002) to  $0.048 g/cm^2$  (7/9/2002), within the EWT range reported in a study that examined the relationship between MSI and EWT (Ceccato et al., 2001). The temporal dynamics of LSWI within the plant-growing season at the Howland site are sensitive to changes of FMC

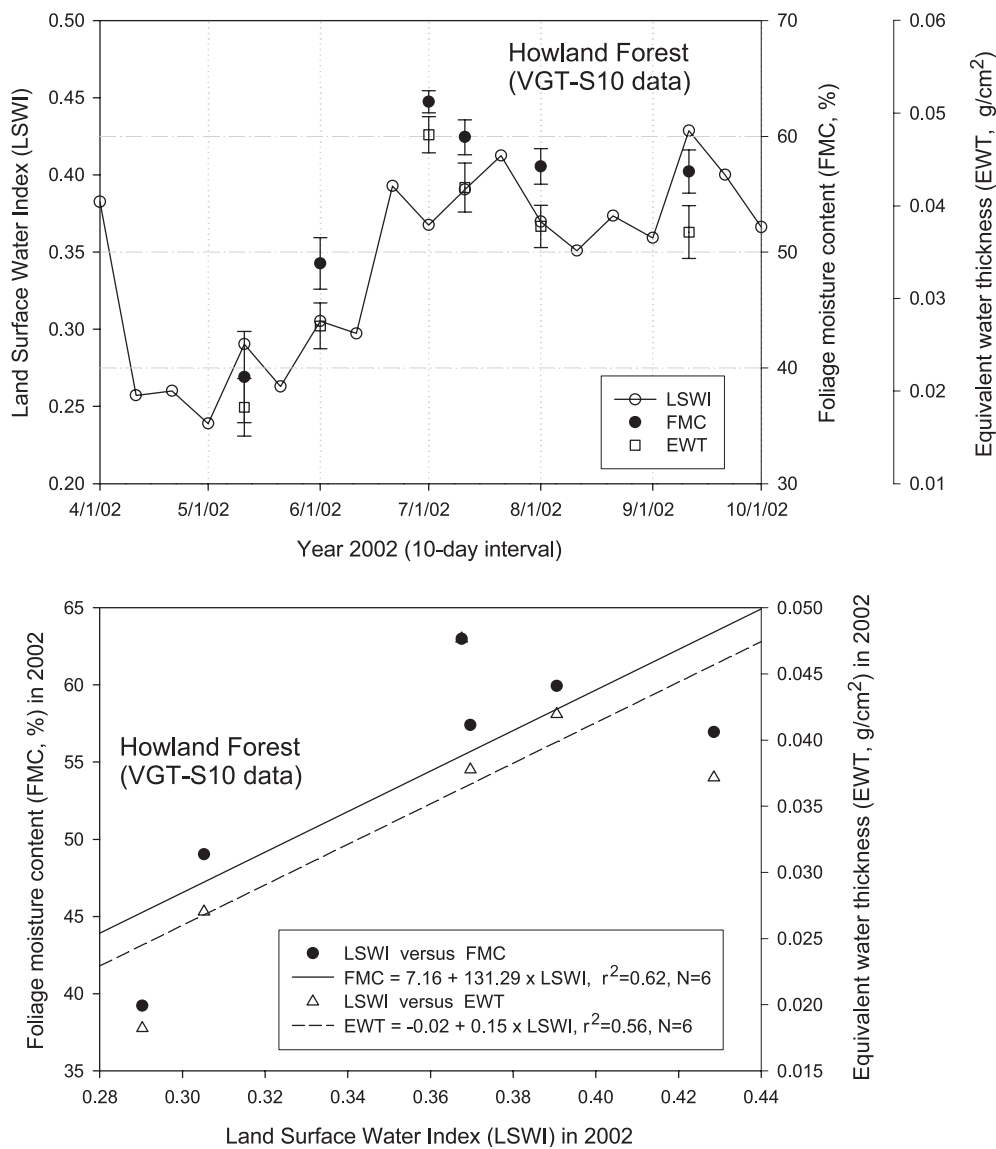


Fig. 8. A comparison between Land Surface Water Index (LSWI) and vegetation water content of forests in 2002 at the flux tower site of Howland Forest, Maine, USA. The error bars for foliage moisture content (FMC, %) and equivalent water thickness (EWT,  $g/cm^2$ ) are the standard deviation of measurements at individual sampling dates. Field measurements of fresh and dry weight were conducted on leaves of two dominant species (red spruce and eastern hemlock) at the Howland site.

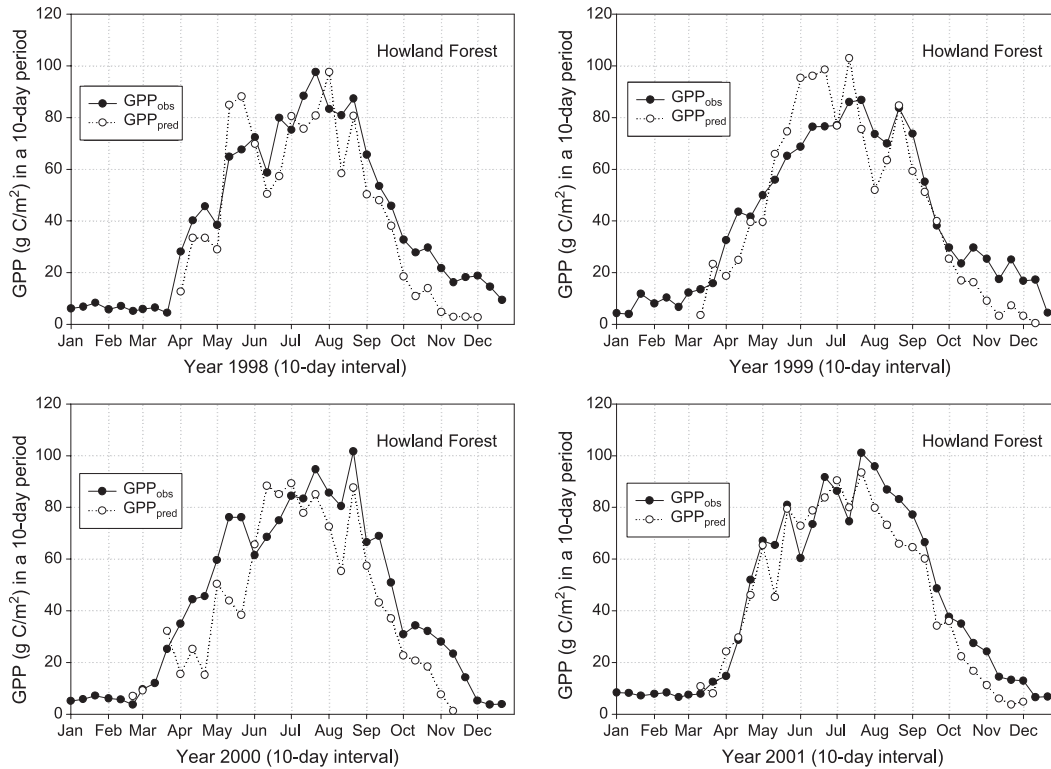


Fig. 9. A comparison of the seasonal dynamics between the observed gross primary production (GPP) and predicted GPP over the photosynthetically active period (April 1 to November 10) during 1998–2001 at the eddy flux tower site of Howland Forest, Maine, USA. Solid circle— $GPP_{obs}$ , and open circle— $GPP_{pred}$ .

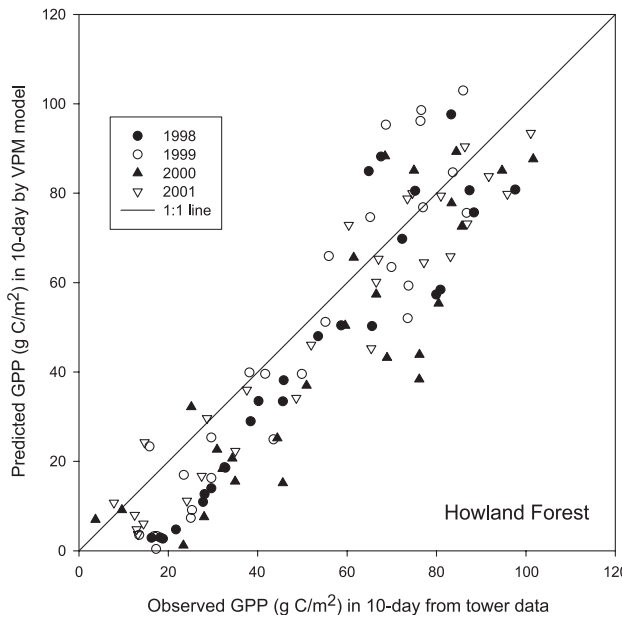


Fig. 10. A comparison between the observed gross primary production (GPP) and predicted GPP over the photosynthetically active period (April 1 to November 10) during 1998–2001 at the eddy flux tower site of Howland Forest, Maine. The simple linear regression models:  $GPP_{pred} = 0.91 \times GP - GPP_{obs}$ ,  $r^2 = 0.95$ ,  $N = 88$ ,  $P < 0.0001$ , or  $GPP_{pred} = -11.63 + 1.08 \times GP - GPP_{obs}$ ,  $r^2 = 0.79$ ,  $N = 88$ ,  $P < 0.0001$ .

and EWT in 2002 (Fig. 8). For future field work at the Howland site, additional field measurement of SLW and LAI should be carried out together with measurements of foliage fresh weight and dry weight, which would lead to improve retrieval of EWT through satellite-based water indices, as demonstrated in recent studies (Ceccato et al., 2001, 2002a,b). As suggested by the limited field data of FMC in 2002 (Fig. 8) and the close relationship between LSWI and MSI during 1998–2001 (Fig. 7) at the Howland site, LSWI might be a useful indicator for canopy water content of evergreen needleleaf forest.

### 5.3. Seasonal dynamics of predicted $CO_2$ fluxes from the VPM model

The VPM model was run using the site-specific data of temperature, PAR and vegetation indices in 1998–2001. The seasonal dynamics of predicted GPP ( $GPP_{pred}$ ) from the VPM model was compared with the observed GPP ( $GPP_{obs}$ ) data at 10-day interval over the period of April 1–November 10 (Fig. 9). The seasonal dynamics of  $GPP_{pred}$  over the plant-growing season agreed reasonably well with those of  $GPP_{obs}$ . The simple linear regression model also shows a good agreement between  $GPP_{pred}$  and  $GPP_{obs}$  during the plant-growing season in 1998–2001 (Fig. 10). Seasonally integrated  $GPP_{pred}$  ( $g C/m^2$ ) over the period of April 1 to November 10 is lower than seasonally integrated  $GPP_{obs}$ , ranging from  $-20\%$  in 2000 to  $-3\%$  in 1999 (Table 1).

## 6. Discussions

The multi-year simulations of the VPM model have shown that in general, there is a good agreement between  $GPP_{pred}$  and  $GPP_{obs}$  over the photosynthetically active period during 1998–2001. However, there still exist large differences between  $GPP_{obs}$  and  $GPP_{pred}$  in a few 10-day periods (Fig. 9), for instance, smaller  $GPP_{pred}$  in early April, and October–November during 1998–2000. Those large discrepancies between  $GPP_{obs}$  and  $GPP_{pred}$  may be attributed to three sources of errors. The first source is the sensitivity of the VPM model to PAR and temperature. Air temperature in October–November is relatively low,  $T_{scalar}$  may be over-corrected (smaller values), resulting in lower light use efficiency ( $\epsilon$ ). Selection of  $T_{min}$  is likely to have some impact on  $T_{scalar}$ , particularly in both early spring and late fall seasons. In this study, we used  $T_{min}=0$  °C (Aber & Federer, 1992), while another process-based ecosystem model used  $T_{min}=-2.0$  °C for temperate forest (Raich et al., 1991). The second source is the error (over-estimation or underestimation) of observed GPP ( $GPP_{obs}$ ).  $GPP_{obs}$  is calculated from field-measured NEE ( $NEE_{obs}$ ) and ecosystem respiration ( $R_{day}$  and  $R_{night}$ ):  $NEE_{obs}=GPP_{obs}-(R_{day}+R_{night})$ . For a given amount of NEE as measured by the eddy-covariance method, an error in estimation of  $R_{day}$  would result in an error in estimation of GPP. The two major steps that must be taken to derive GPP are the gap filling of NEE and estimation of daytime ecosystem respiration. Both of these steps require subjective decisions and are currently the subject of a great deal of discussion (Falge et al., 2001a,b). The third source is the time-series data of vegetation indices derived from satellite images. We used the 10-day VGT composites that have no BRDF correction or normalization, and thus, the effect of angular geometry on surface reflectance and vegetation indices remained. The NDVI-based compositing method used to generate the 10-day composite VGT image may also affect the time-series data of vegetation indices (EVI and LSWI). Use of daily cloud-free VGT data may improve prediction of GPP by the VPM model. Further investigations are needed to quantify the relative role of individual sources of error in evaluation of the VPM model using  $CO_2$  flux data from flux tower sites.

In the VPM model, we propose two simple but innovative ideas that could result in significant improvement in estimating seasonal dynamics of gross primary production of evergreen needleleaf forests at large spatial scales. The first hypothesis in the VPM model is to use an improved vegetation index (e.g., EVI in this study) to estimate the fraction of PAR absorbed by photosynthetically active vegetation (PAV) for photosynthesis ( $FAPAR_{PAV}$ ), which clearly differ from the other PEM models that use NDVI to estimate FAPAR (Potter et al., 1993; Prince & Goward, 1995; Running et al., 2000). Quantitative partition of vegetation canopy into PAV and NPV components, and consequently partition of FAPAR into  $FAPAR_{PAV}$  and

$FAPAR_{NPV}$  are important, and a laboratory-based study was conducted to estimate canopy photosynthetic and non-photosynthetic components from spectral transmittance (Serrano et al., 2000a). EVI is a semi-empirical mathematical transformation of observed reflectance from individual spectral bands (blue, red and NIR) of optical sensors (Huete et al., 2002). The seasonal dynamics of EVI agreed well with the observed GPP of evergreen needleleaf forest in 1998–2001, but NDVI had poor correlation with GPP of evergreen needleleaf forest during the plant-growing season (Fig. 6). Another study also reported that canopy NDVI did not correlated with leaf net  $CO_2$  uptake of mature evergreen chaparral shrubs in 1998–1999 (Stylinski et al., 2002). One interpretation of the observed decrease of EVI during late summer and fall seasons is that less amount of PAR is absorbed by the PAV for photosynthesis due to the aging process of leaves (possibly an increase of NPV within leaves, changes in leaf structure and pigments). Ongoing measurements in the California chaparral suggest that evergreen shrubs undergo large seasonal changes in their leaf carotenoid/chlorophyll ratios (Sims & Gamon, 2002). More field and laboratory studies across leaf, canopy and landscape levels are needed to better understand and quantify the relationship between improved vegetation indices (e.g., EVI) and  $FAPAR_{PAV}$  of forests in the plant-growing season. In addition, progress has recently been made in using radiative transfer modeling approach to develop advanced vegetation indices for estimation of FAPAR, using the top-of-atmosphere (TOA) reflectance data from the VGT sensor (Gobron et al., 2000). When the TOA reflectance data from the VGT sensor become freely available to users, it will be of interest to compare those advanced vegetation indices (Gobron et al., 2000) with the semi-empirical EVI, using  $CO_2$  flux data from the flux tower sites.

The second hypothesis in the VPM model is to use a satellite-based water index for estimating the water scalar ( $W_{scalar}$ ) in calculation of light use efficiency ( $\epsilon$ ). This alternative approach differs from other PEM models that use soil moisture and/or water vapor pressure deficit to adjust the water scalar ( $W_{scalar}$ ) in calculation of light use efficiency ( $\epsilon$ ) (Field et al., 1995; Prince & Goward, 1995; Running et al., 2000). To what degree canopy water content can be retrieved from satellite images is an important research question for remote sensing science (Champagne et al., 2003; Penuelas et al., 1997; Sims & Gamon, 2003). While the best wavelength for prediction of canopy water content from ground-based data (no atmospheric interference) were 960 and 1180 nm, the best wavelength for satellite remote sensing of canopy water content (with atmospheric interference) would be 1150–1260 and 1520–1540 nm (Sims & Gamon, 2003). The availability of time-series data of SWIR and NIR bands from the new generation of optical sensors (e.g., VGT, MODIS) offers new opportunity for quantifying canopy water content at large spatial scales through both the vegetation indices

approach (Ceccato et al., 2002b) and the radiative transfer modeling approach (Zarco-Tejada et al., 2003). Earlier studies have shown that the Moisture Stress Index (MSI) and the Global Vegetation Moisture Index (VGMI) are sensitive to changes in equivalent water thickness ( $\text{g}/\text{cm}^2$ ) at leaf and canopy levels (Ceccato et al., 2001, 2002a,b; Hunt & Rock, 1989). A water index calculated as a normalized difference between MODIS band 6 (1628–1652 nm) and band 2 (841–876 nm) was compared to in situ top layer soil moisture measurement from the semiarid Senegal and the results showed a strong correlation between the water index and soil moisture in 2001 (Fensholt & Sandhol, 2003). The preliminary comparison between LSWI and foliage moisture content of evergreen needleleaf forest at Howland Forest, Maine (Fig. 8) has shown the seasonal changes of leaf water content and sensitivity of LSWI in the plant-growing season. More fieldwork are needed to collect multiple-year data of leaf and canopy water content of evergreen needleleaf forests over the plant-growing season, in support of the effort to retrieve canopy water content through both the empirical and radiative transfer modeling approaches. In addition to improving quantification of the accuracy, adequacy and precision of water indices (e.g., LSWI), more field and laboratory work are also needed to study the effect of leaf and canopy water content on photosynthesis of evergreen needleleaf forests, so that our hypothesis about the relationship between leaf water content and photosynthesis in the VPM model could be fully tested at the canopy level and over the plant-growing season.

## 7. Summary

The Howland Forest site is representative of an ecotonal boreal-northern hardwood transitional forest (Hollinger et al., 1999). The eddy covariance measurements have shown that evergreen needleleaf forest at the site had distinct seasonal dynamics and moderate interannual variation in GPP during 1998–2001. The response functions of  $\text{CO}_2$  and water vapor exchange at Howland Forest due to climate variation are similar to those of other spruce forests (Goulden et al., 1997; Hollinger et al., 1999). The satellite-based VPM model uses two improved vegetation indices (EVI and LSWI) that can be generated only from the new generation of optical sensors (e.g., VGT), which has the potential to provide major improvement over the current satellite-based Production Efficiency Models that only employ NDVI. The VPM model is capable of tracking seasonal dynamics and interannual variations in GPP of evergreen needleleaf forest at a sub-monthly (10-day in this study) temporal resolution. Additional studies are needed to continue validation of the VPM model across various forest tower sites, that is, cross-biome comparison and cross-site comparison within a biome type. Calculation of GPP is the first step in the study of carbon cycle of terrestrial ecosystems. Our progress in

satellite-based modeling of GPP may have significant implications on the study of carbon cycle processes of evergreen needleleaf forests in both temperate and boreal zones. As the VGT sensor provides daily images of the globe, there is a potential to use the VPM model and climate data (temperature and PAR) to quantify the spatial patterns and temporal dynamics of GPP of boreal forests at 1-km spatial resolution.

## Acknowledgements

We thank the International Paper for providing access to the research site in Howland, Maine, USA. John Lee, Holly Hughes, and Jeremiah Walsh provided expert assistance with the multi-year  $\text{CO}_2$  flux and climate data set for the Howland Forest site (<http://public.ornl.gov/ameriflux/Data/index.cfm>). We are grateful to the four reviewers, and their comments and suggestions on the earlier versions of the manuscript greatly improved the manuscript. The  $\text{CO}_2$  flux research at the Howland site was supported by the Office of Science (BER), U.S. Department of Energy, through the Northeast Regional Center of the National Institute for Global Environmental Change under Cooperative Agreement No. DE-FC03-90ER61010. The modeling study was supported by research grants from NASA Interdisciplinary Science Program (NAG5-10135) and Land Cover and Land Use Change Program (NAG5-11160).

## References

- Aber, J. D., & Federer, C. A. (1992). A generalized, lumped-parameter model of photosynthesis, evapotranspiration and net primary production in temperate and boreal forest ecosystems. *Oecologia*, *92*, 463–474.
- Aber, J. D., Reich, P. B., & Goulden, M. L. (1996). Extrapolating leaf  $\text{CO}_2$  exchange to the canopy: A generalized model of forest photosynthesis compared with measurements by eddy correlation. *Oecologia*, *106*, 257–265.
- Asner, G. P., Wessman, C. A., & Archer, S. (1998). Scale dependence of absorption of photosynthetically active radiation in terrestrial ecosystems. *Ecological Applications*, *8*, 1003–1021.
- Behrenfeld, M. J., Randerson, J. T., McClain, C. R., Feldman, G. C., Los, S. O., Tucker, C. J., Falkowski, P. G., Field, C. B., Frouin, R., Esaias, W. E., Kolber, D. D., & Pollack, N. H. (2001). Biospheric primary production during an ENSO transition. *Science*, *291*, 2594–2597.
- Boegh, E., Soegaard, H., Broge, N., Hasager, C. B., Jensen, N. O., Schelde, K., & Thomsen, A. (2002). Airborne multispectral data for quantifying leaf area index, nitrogen concentration, and photosynthetic efficiency in agriculture. *Remote Sensing of Environment*, *81*, 179–193.
- Ceccato, P., Flasse, S., & Gregoire, J. M. (2002a). Designing a spectral index to estimate vegetation water content from remote sensing data: Part 2. Validation and applications. *Remote Sensing of Environment*, *82*, 198–207.
- Ceccato, P., Flasse, S., Tarantola, S., Jacquemoud, S., & Gregoire, J. M. (2001). Detecting vegetation leaf water content using reflectance in the optical domain. *Remote Sensing of Environment*, *77*, 22–33.
- Ceccato, P., Gobron, N., Flasse, S., Pinty, B., & Tarantola, S. (2002b). Designing a spectral index to estimate vegetation water content from

- remote sensing data: Part I. Theoretical approach. *Remote Sensing of Environment*, 82, 188–197.
- Champagne, C. M., Staenz, K., Bannari, A., McNairn, H., & Deguise, J.-C. (2003). Validation of a hyperspectral curve-fitting model for estimation of plant water content of agricultural canopies. *Remote Sensing of Environment*, 87, 148–160.
- DeLucia, E. H., & Smith, W. K. (1987). Air and soil temperature limitations on photosynthesis in Englemann spruce during summer. *Canadian Journal of Forest Research*, 17, 527–533.
- Falge, E., Baldocchi, D., Olson, R., Anthoni, P., Aubinet, M., Bernhofer, C., Burba, G., Ceulemans, G., Clement, R., Dolman, H., Granier, A., Gross, P., Grunwald, T., Hollinger, D., Jensen, N. O., Katul, G., Keronen, P., Kowalski, A., Lai, C. T., Law, B. E., Meyers, T., Moncrieff, J., Moors, E., Munger, J. W., Pilegaard, K., Rannik, U., Rebmann, C., Suyker, A., Tenhunen, J., Tu, K., Verma, S., Vesala, T., Wilson, K., & Wofsy, S. (2001a). Gap filling strategies for long term energy flux data sets. *Agricultural and Forest Meteorology*, 107, 71–77.
- Falge, E., Baldocchi, D., Olson, R., Anthoni, P., Aubinet, M., Bernhofer, C., Burba, G., Ceulemans, R., Clement, R., Dolman, H., Granier, A., Gross, P., Grunwald, T., Hollinger, D., Jensen, N. O., Katul, G., Keronen, P., Kowalski, A., Lai, C. T., Law, B. E., Meyers, T., Moncrieff, H., Moors, E., Munger, J. W., Pilegaard, K., Rannik, U., Rebmann, C., Suyker, A., Tenhunen, J., Tu, K., Verma, S., Vesala, T., Wilson, K., & Wofsy, S. (2001b). Gap filling strategies for defensible annual sums of net ecosystem exchange. *Agricultural and Forest Meteorology*, 107, 43–69.
- Fensholt, R., & Sandhol, I. (2003). Derivation of a shortwave infrared water stress index from MODIS near- and shortwave infrared data in a semiarid environment. *Remote Sensing of Environment*, 87, 111–121.
- Field, C. B., Behrenfeld, M. J., Randerson, J. T., & Falkowski, P. (1998). Primary production of the biosphere: Integrating terrestrial and oceanic components. *Science*, 281, 237–240.
- Field, C. B., Randerson, J. T., & Malmstrom, C. M. (1995). Global net primary production—combining ecology and remote-sensing. *Remote Sensing of Environment*, 51, 74–88.
- Frolking, S. E., Bubier, J. L., Moore, T. R., Ball, T., Bellisario, L. M., Bhardwaj, A., Carroll, P., Crill, P. M., Lafleur, P. M., McCaughey, J. H., Roulet, N. T., Suyker, A. E., Verma, S. B., Waddington, J. M., & Whiting, G. J. (1998). Relationship between ecosystem productivity and photosynthetically active radiation for northern peatlands. *Global Biogeochemical Cycles*, 12, 115–126.
- Gao, B. C. (1996). NDWI—A normalized difference water index for remote sensing of vegetation liquid water from space. *Remote Sensing of Environment*, 58, 257–266.
- Gobron, N., Pinty, B., Verstraete, M., & Govaerts, Y. (1999). The MERIS Global Vegetation Index (MGVI): Description and preliminary application. *International Journal of Remote Sensing*, 20, 1917–1927.
- Gobron, N., Pinty, B., Verstraete, M. M., & Widlowski, J. L. (2000). Advanced vegetation indices optimized for up-coming sensors: Design, performance, and applications. *IEEE Transactions on Geoscience and Remote Sensing*, 38, 2489–2505.
- Goulden, M. L., Daube, B. C., Fan, S. M., Sutton, D. J., Bazzaz, A., Munger, J. W., & Wofsy, S. C. (1997). Physiological responses of a black spruce forest to weather. *Journal of Geophysical Research-Atmospheres*, 102, 28987–28996.
- Govaerts, Y. M., Verstraete, M. M., Pinty, B., & Gobron, N. (1999). Designing optimal spectral indices: A feasibility and proof of concept study. *International Journal of Remote Sensing*, 20, 1853–1873.
- Hollinger, D. Y., Goltz, S. M., Davidson, E. A., Lee, J. T., Tu, K., & Valentini, H. T. (1999). Seasonal patterns and environmental control of carbon dioxide and water vapour exchange in an ecotonal boreal forest. *Global Change Biology*, 5, 891–902.
- Huete, A., Didan, K., Miura, T., Rodriguez, E. P., Gao, X., & Ferreira, L. G. (2002). Overview of the radiometric and biophysical performance of the MODIS vegetation indices. *Remote Sensing of Environment*, 83, 195–213.
- Huete, A. R., Liu, H. Q., Batchily, K., & vanLeeuwen, W. (1997). A comparison of vegetation indices global set of TM images for EOS-MODIS. *Remote Sensing of Environment*, 59, 440–451.
- Hunt, E. R., & Rock, B. N. (1989). Detection of changes in leaf water-content using near-infrared and middle-infrared reflectances. *Remote Sensing of Environment*, 30, 43–54.
- Justice, C. O., Vermote, E., Townshend, J. R. G., Defries, R., Roy, D. P., Hall, D. K., Salomonson, V. V., Privette, J. L., Riggs, G., Strahler, A., Lucht, W., Myneni, R. B., Knyazikhin, Y., Running, S. W., Nemani, R. R., Wan, Z. M., Huete, A. R., van Leeuwen, W., Wolfe, R. E., Giglio, L., Muller, J. P., Lewis, P., & Barnsley, M. J. (1998). The Moderate Resolution Imaging Spectroradiometer (MODIS): Land remote sensing for global change research. *IEEE Transactions on Geoscience and Remote Sensing*, 36, 1228–1249.
- Law, B. E., Falge, E., Gu, L., Baldocchi, D. D., Bakwin, P., Berbigier, P., Davis, K., Dolman, A. J., Falk, M., Fuentes, J. D., Goldstein, A., Granier, A., Grelle, A., Hollinger, D., Janssens, I. A., Jarvis, P., Jensen, N. O., Katul, G., Mahli, Y., Matteucci, G., Meyers, T., Monson, R., Munger, W., Oechel, W., Olson, R., Pilegaard, K., Paw, K. T., Thorgerisson, H., Valentini, R., Verma, S., Vesala, T., Wilson, K., & Wofsy, S. (2002). Environmental controls over carbon dioxide and water vapor exchange of terrestrial vegetation. *Agricultural and Forest Meteorology*, 113, 97–120.
- Law, B. E., Waring, R. H., Anthoni, P. M., & Aber, J. D. (2000). Measurements of gross and net ecosystem productivity and water vapour exchange of a *Pinus ponderosa* ecosystem, and an evaluation of two generalized models. *Global Change Biology*, 6, 155–168.
- Malmstrom, C. M., Thompson, M. V., Juday, G. P., Los, S. O., Randerson, J. T., & Field, C. B. (1997). Interannual variation in global-scale net primary production: Testing model estimates. *Global Biogeochemical Cycles*, 11, 367–392.
- Melillo, J. M., McGuire, A. D., Kicklighter, D. W., Moore, B., Vorosmarty, C. J., & Schloss, A. L. (1993). Global climate-change and terrestrial net primary production. *Nature*, 363, 234–240.
- Penuelas, J., Pinol, J., Ogaya, R., & Filella, I. (1997). Estimation of plant water concentration by the reflectance water index WI (R900/R700). *International Journal of Remote Sensing*, 18, 2869–2875.
- Potter, C. S., Randerson, J. T., Field, C. B., Matson, P. A., Vitousek, P. M., Mooney, H. A., & Klooster, S. A. (1993). Terrestrial ecosystem production—a process model-based on global satellite and surface data. *Global Biogeochemical Cycles*, 7, 811–841.
- Prince, S. D., & Goward, S. N. (1995). Global primary production: A remote sensing approach. *Journal of Biogeography*, 22, 815–835.
- Raich, J. W., Rastetter, E. B., Melillo, J. M., Kicklighter, D. W., Steudler, P. A., Peterson, B. J., Grace, A. L., Moore, B., & Vorosmarty, C. J. (1991). Potential net primary productivity in South-America—application of a global-model. *Ecological Applications*, 1, 399–429.
- Rock, B. N., Williams, D. L., Moss, D. M., Lauten, G. N., & Kim, M. (1994). High-spectral-resolution field and laboratory optical reflectance measurements of red spruce and eastern hemlock needles and branches. *Remote Sensing of Environment*, 47, 176–189.
- Ruimy, A., Dedieu, G., & Saugier, B. (1996). TURC: A diagnostic model of continental gross primary productivity and net primary productivity. *Global Biogeochemical Cycles*, 10, 269–285.
- Ruimy, A., Jarvis, P. G., Baldocchi, D. D., & Saugier, B. (1995). CO<sub>2</sub> fluxes over plant canopies and solar radiation: A review. *Advances in Ecological Research*, 1–68.
- Ruimy, A., Kerger, L., & Bondeau, A. (1999). Comparing global models of terrestrial net primary productivity (NPP): Analysis of differences in light absorption and light-use efficiency. *Global Change Biology*, 5, 56–64.
- Ruimy, A., Saugier, B., & Dedieu, G. (1994). Methodology for the estimation of terrestrial net primary production from remotely sensed data. *Journal of Geophysical Research, D: Atmospheres*, 99, 5263–5283.
- Running, S. W., Nemani, R., Glassy, J. M., & Thornton, P. (1999). MODIS Daily photosynthesis (PSN) and annual net primary production (NPP) product (MOD17). Algorithm Theoretical Basis Document, Version 3.0, April 29, 1999.

- Running, S. W., Thornton, P. E., Nemani, R., & Glassy, J. M. (2000). Global terrestrial gross and net primary productivity from the Earth Observing System. In O. E. Sala, R. B. Jackson, H. A. Mooney, & R. W. Howarth (Eds.), *Methods in ecosystem science* (pp. 44–57). New York: Springer.
- Schulze, E. D., Lloyd, J., Kelliher, F. M., Wirth, C., Rebmann, C., Luhker, B., Mund, M., Knohl, A., Milyukova, I. M., Schulze, W., Ziegler, W., Varlagin, A. B., Sogachev, A. F., Valentini, R., Dore, S., Grigoriev, S., Kolle, O., Panfyorov, M. I., Tchebakova, N., & Vygodskaya, N. N. (1999). Productivity of forests in the Eurosiberian boreal region and their potential to act as a carbon sink—a synthesis. *Global Change Biology*, 5, 703–722.
- Serrano, L., Gamon, J. A., & Penuelas, J. (2000a). Estimation of canopy photosynthetic and nonphotosynthetic components from spectral transmittance. *Ecology*, 81, 3149–3162.
- Serrano, L., Ustin, S. L., Roberts, D. A., Gamon, J. A., & Penuelas, J. (2000b). Deriving water content of chaparral vegetation from AVIRIS data. *Remote Sensing of Environment*, 74, 570–581.
- Sims, D. A., & Gamon, J. A. (2002). Relationships between leaf pigment content and spectral reflectance across a wide range of species, leaf structures and developmental stages. *Remote Sensing of Environment*, 81, 337–354.
- Sims, D. A., & Gamon, J. A. (2003). Estimation of vegetation water content and photosynthetic tissue area from spectral reflectance: A comparison of indices based on liquid water and chlorophyll absorption features. *Remote Sensing of Environment*, 84, 526–537.
- Stylinski, C. D., Gamon, J. A., & Oechel, W. C. (2002). Seasonal patterns of reflectance indices, carotenoid pigments and photosynthesis of evergreen chaparral species. *Oecologia*, 131, 366–374.
- Sullivan, J. H., Bovard, B. D., & Middleton, E. M. (1997). Variability in leaf-level CO<sub>2</sub> and water fluxes in *Pinus banksiana* and *Picea mariana* in Saskatchewan. *Tree Physiology*, 17, 553–561.
- Tucker, C. J. (1979). Red and photographic infrared linear combinations for monitoring vegetation. *Remote Sensing of Environment*, 8, 127–150.
- Tucker, C. J. (1980). Remote-sensing of leaf water-content in the near-infrared. *Remote Sensing of Environment*, 10, 23–32.
- Turner, D. P., Urbanski, S., Bremer, D., Wofsy, S. C., Meyers, T., Gower, S. T., & Gregory, M. (2003). A cross-biome comparison of daily light use efficiency for gross primary production. *Global Change Biology*, 9, 383–395.
- Weiss, A., & Norman, J. M. (1985). Partitioning solar-radiation into direct and diffuse, visible and near-infrared components. *Agricultural and Forest Meteorology*, 34, 205–213.
- Wilson, K. B., Baldocchi, D. D., & Hanson, P. J. (2001). Leaf age affects the seasonal patterns of photosynthetic capacity and net ecosystem exchange of carbon in a deciduous forest. *Plant, Cell and Environment*, 24, 571–583.
- Xiao, X., Boles, S., Frolking, S., Salas, W., Moore, B., Li, C., He, L., & Zhao, R. (2002a). Landscape-scale characterization of cropland in China using Vegetation and Landsat TM images. *International Journal of Remote Sensing*, 23, 3579–3594.
- Xiao, X., Boles, S., Frolking, S., Salas, W., Moore, B., Li, C., He, L., & Zhao, R. (2002b). Observation of flooding and rice transplanting of paddy rice fields at the site to landscape scales in China using VEGETATION sensor data. *International Journal of Remote Sensing*, 23, 3009–3022.
- Xiao, X., Boles, S., Liu, J. Y., Zhuang, D. F., & Liu, M. L. (2002c). Characterization of forest types in Northeastern China, using multi-temporal SPOT-4 VEGETATION sensor data. *Remote Sensing of Environment*, 82, 335–348.
- Xiao, X., Braswell, B., Zhang, Q., Boles, S., Frolking, S., & Moore, B. (2003). Sensitivity of vegetation indices to atmospheric aerosols: Continental-scale observations in Northern Asia. *Remote Sensing of Environment*, 84, 385–392.
- Zarco-Tejada, P. J., Rueda, C. A., & Ustin, S. L. (2003). Water content estimation in vegetation with MODIS reflectance data and model inversion methods. *Remote Sensing of Environment*, 85, 109–124.